ChemComm

Accepted Manuscript

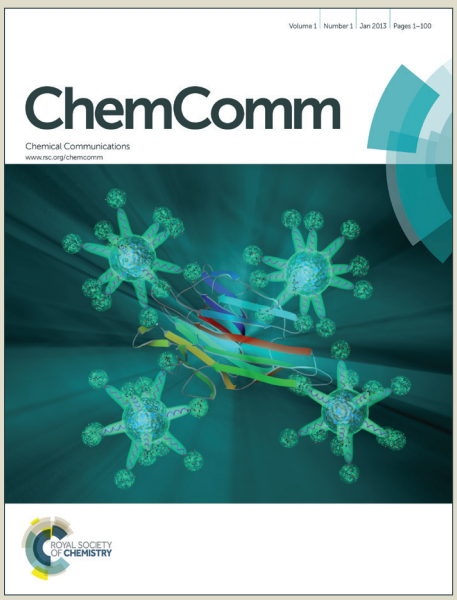

ROYAL SOCIETY OF CHEMISTRY

www.rsc.org/chemcomm

ChemComm

COMMUNICATION

Solution-based fabrication of a highly catalytically active 3D network constructed from 1D metal-organic framework-coated polymeric worm-like micelles†

Received 00th January 20xx,
Accepted 00th January 20xx

DOI: 10.1039/x0xx00000x

www.rsc.org/

Junqi Yi, Haodong Li, Li Jiang, Kaka Zhang and Daoyong Chen*

A 3D network constructed from metal-organic framework composite nanowires with a uniform width and a loose (swollen) structure has been prepared. It contained micro-, meso- and macro-pores, which make the 3D network ideal for use as a catalyst, as evidenced by its high catalytic activity in the Knoevenagel reaction.

Metal-organic frameworks (MOFs) or porous coordination polymers (PCPs) are porous materials constructed through the assembly of metal ions and organic ligands.[1] These materials with crystalline structures exhibit high surface area, high porosity, chemical tunability and diverse functionality. Because of these characteristics, MOFs have strong potential for use in applications such as gas storage,[2] air purification,[3] separation,[4] catalysis,[5] and sensing.[6] Although the intrinsic micropores result in a large specific surface area, their small size limits molecular diffusion and access by large molecules. The MOFs with a large specific external surface area and the external surface being fully exposed are highly desirable.[Note 1] One approach to such MOFs is to prepare MOF nanocrystals.[7] In most cases, MOF nanocrystals must be collected and purified through solvent washing and then activated in a bulk state before use. The nanocrystals will fuse together after these treatments because they have a strong tendency to fuse with each other due to the inter-particle interaction between the unsaturated metal ions and the ligands on the external surface.[8] The fusion results in a considerable decrease in their external surface area and in the continuity of their packing pores. Alternatively, mesopores and macropores can be introduced into large MOF crystals to form hierarchical porous structures; these hierarchical structures decrease the path length for transport of small molecules in the micropores and increase the external surface area accessible to large molecules or multiple-molecule reactions. However, because of the relatively weak interaction of the coordination bonds between metal ions and ligands in MOFs, conventional methods such as using surfactants as porogens did not work well.[9] The preparation of mesoporous MOFs remain challenging, and few related studies have been reported.[7f, 10]

Herein, we report the large-scale fabrication of a 3D network constructed from composite nanowires with uniform width formed by an integrated ZIF-8 crystal layer coating the surface of polymeric worm-like micelles (PWs) (scheme 1). ZIF-8 is a prototypical MOF composed of Zn^{2+} ions and 2-methylimidazole,[11] and the PWs had a poly(ethylene glycol) (PEG) shell and a slightly crosslinked poly(4-vinylpyridine) (P4VP) core. The 3D network was prepared by crystallization of ZIF-8 on the surface of the PWs in suspension at a relatively high PW concentration. The crystallization yielded composite nanowires and meanwhile crosslinked them to form the 3D network. Because the individual composite nanowires were dispersible in the suspension, the 3D network had a loose (swollen) structure, containing micropores of ZIF-8, mesopores formed by gaps between neighboring nanocrystals on ZIF-8 crystal layer and the stacking macropores through which the external surface of the composite nanowires was fully exposed. When used to catalyze the Knoevenagel reaction between benzaldehyde and malononitrile,[12] the 3D network with this hierarchical porous structure exhibited substantially greater catalytic activity compared to pure ZIF-8 nanocrystals and microcrystals.

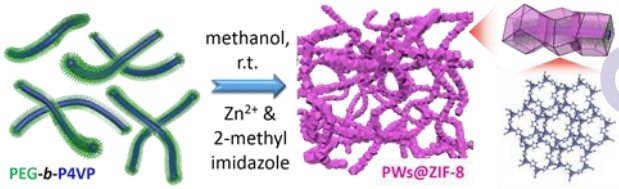

Scheme 1. Illustration of the preparation of 3D network

The PWs with a PEG shell and a slightly crosslinked (crosslinking degree 10%) P4VP core (diameter about 28 nm) were prepared in large scale through self-assembly of DNA

The State Key Laboratory of Molecular Engineering of Polymers
Department of Macromolecular Science
Fudan University
Handan Road 220, Shanghai 200433, P. R. China
E-mail: chendy@fudan.edu.cn
† Electronic Supplementary Information (ESI) available. See
DOI: 10.1039/x0xx00000x

PEG_{113}-*b*-$P4VP_{118}$ micelles on the basis of the method developed in our laboratory (S2 in the ESI).[13] The 3D network was prepared by mixing PWs with zinc nitrate hexahydrate (Zn^{2+}) and 2-methylimidazole (Hmim), the precursors of ZIF-8, in methanol at room temperature (S3 in the ESI). After 24 hours of incubation, the final floccule-like precipitate was collected by centrifugation and washed three times with methanol. FESEM observations (Figures 1a-b, Figure S2a-e) demonstrated that the product is a 3D network constructed from curved nanowires with a uniform width of approximately 60 nm, which is much greater than the width of the PWs (28 nm). A TEM image at greater magnification and electron diffraction experiment (Figure 1c-d) revealed that the structure of the nanowires comprised a ZIF-8 crystal layer encapsulating the PWs; we further confirmed this structure by preparing the composite nanowires encapsulating Au nanoparticles within the P4VP core of the PWs (Figure 1e). The composite nanowires were formed through crystallization of ZIF-8 directed by the PWs as the template. Our control experiments indicated that PWs were effective templates on which the ZIF-8 prefers nucleation and the crystallization of ZIF-8 onto the surface of the PWs primarily resulted from the interaction between Zn^{2+} and the PEG shell (S5 in the ESI). The sizes of the stacking macropores were clearly observed in the FESEM images. A large part of the macropores were in the range between 300 and 900 nm (Figure S2e, Figure 2d), which is close to the lengths of the composite nanowires (Table S1). Detailed inspection of the 3D network's structure revealed that (Figure 1a-b, Figure S2) the pores were much larger than the voids that could be formed by close-packing of the nanowires that were primarily less than 1 μm. Insolubility-induced aggregation of the composite nanowires into the 3D network was excluded on the basis of the fact that individual composite nanowires at the same concentration in a suspension without the ZIF-8 precursors were individually dispersed (S6 in the ESI, The zeta potential of the composite nanowires was as high as +60 mV which provides sufficient electric repulsion among the individual composite nanowires for their dispersion). Therefore, we believe that the crosslinking of the dispersible composite nanowires led to the 3D network with the macropores, as evidenced by the crosslink points observed in the FESEM images (indicated by the red arrows in Figure 1b); at the crosslinking points, fusion between the ZIF-8 crystal layers of different nanowires was observed (the inset in Figure 1b). During the formation of the composite nanowires in methanol, precursors first assemble to form ZIF-8 primary particles on the surface of the PWs. Since the primary particles have a strong tendency to fuse together to form larger particles,[14] the fusion between the primary nanoparticles on the different nanowires occurred simultaneously, leading to the crosslinking. Crosslinking limited further close-packing of the nanowires during the processes of purification and activation. These effects guarantee a loose structure of the 3D network. The collected product was dried under vacuum and further activated at 120 °C to form the bulk material. FESEM results show that the 3D network maintained this loose structure in its bulk state after the treatments (

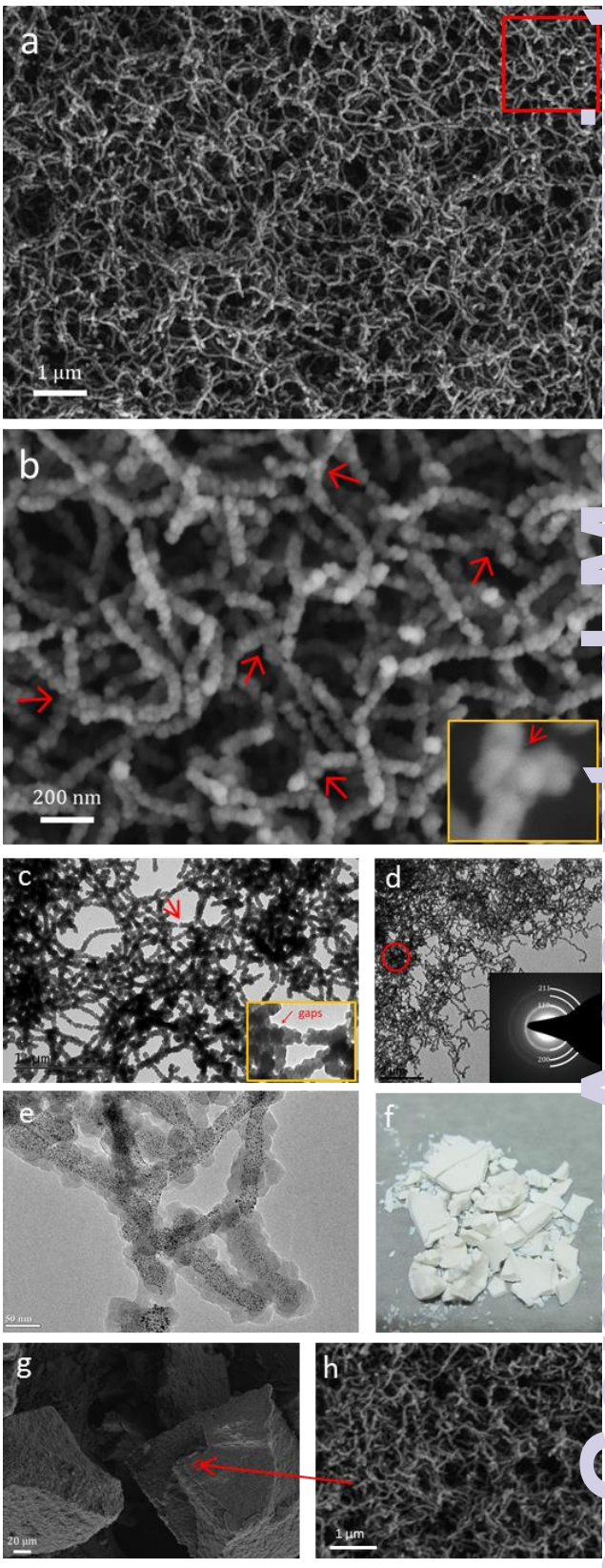

Figure 1. a-d) FESEM and TEM images of the 3D network: (b) is the magnification of th region shown by the red square in (a); inset of (c) is magnification of the region shown by the red arrow; inset of (d) is the SAED pattern taken from the circled region. e) TEM image of the PW-Au composite network; Au nanoparticles located in the P4VP core of PWs were encapsulated into ZIF-8 with the PWs. f-h) Photograph and FESEM images o the bulk-state 3D network after drying and activation.

Figures 1f-h, Figure S2f-g). The product was produced in gram quantities (Figure 1f), indicating that this method can be used for large-scale preparation.

The 3D network after the activation was characterized by thermogravimetric analysis (TGA), powder X-ray diffraction (PXRD), and nitrogen-sorption isotherm and mercury intrusion porosimetry (MIP) measurements. The TGA results indicated that the initial decomposition temperature of the composite nanowires was 250 °C (Figure 2a), identical to that of the PWs. The weight content of the PWs in the 3D network was determined by TGA to be ca. 20%. On the basis of the starting PW amount and the amount contained in the final product, 93% of the PWs in the feed were transferred to the composite nanowires that made up the 3D network. In the powder X-ray diffraction (PXRD) pattern of the 3D network (Figure 2b), the sharp diffraction lines revealed that the composites had a crystal structure typical of ZIF-8 and the crystallinity was perfect. The nitrogen-sorption isotherm measurements (Figure 2c) for the 3D network displayed a type I isotherm that indicated excellent N_2 uptake at low relative pressures ($P/P_0 < 0.1$), which was attributed to the micropores of ZIF-8 (Figure S9). Compared to the N_2 uptake of the pure ZIF-8 crystals, the uptake of the 3D network in this region decreased by approximately 20% (from 415 to 335 cm^3g^{-1}), consistent with the PW content (w.t.%). Therefore, all of the ZIF-8 components crystalized to form the microspores, and the PWs didn't block the pores.[7b] At medium relative pressures ($0.4 < P/P_0 < 0.8$), the type-H4 hysteresis loop (the inset in Figure 2c) indicates the existence of slit-like mesopores.[15] The mesopores are gaps observed by TEM and FESEM (the inset in Figure 1c, Figure S2 a-d and Figure S3). ZIF-8 has a strong tendency to maintain its crystal form (rhombic dodecahedra) during growth, but during the formation of the composite nanowires, it must grow along the PWs. The balance between these two tendencies resulted in gaps between neighboring nanocrystals of ZIF-8 crystal layer. It has also been observed in numerous other studies in which a template was used to direct ZIF-8 crystal growth.[16] The isotherm of the 3D network in the high relative pressure ($P/P_0 > 0.8$) region indicated the presence of stacking mesopores and macropores, which were also detected in aggregates of the ZIF-8 nanocrystals (Figure 2c).[7e, 17] It is notable that the nitrogen-sorption measurements can only detect the macropores of relatively small size (below 100 nm). The pore size distribution curves in the 3D network and ZIF-8 nanocrystals were further measured through mercury intrusion porosimetry (Figure 2d). The 3D network contained a large number of macropores with sizes greater than 100 nm, which is consistent with the FESEM observations; ZIF-8 nanocrystals in the bulk state only contained mesopores and small macropores with diameters less than 100 nm.

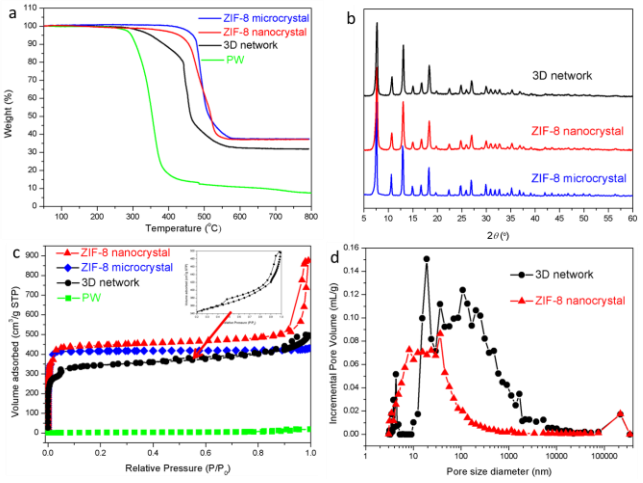

Figure 2. a) TGA curves of the PWs, the 3D network and pure ZIF-8 nanocrystal (65 nm) and microcrystals (1 μm) b) PXRD patterns of the 3D network, ZIF-8 nano- and micro-crystals. c) Nitrogen-sorption isotherms for the PWs, the 3D network, ZIF-8 nano- and microcrystals. d) The pore-size distribution in the 3D network and ZIF-8 nanocrystals, as measured by mercury intrusion porosimetry.

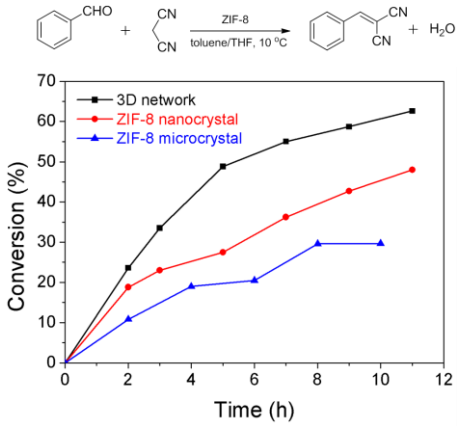

Figure 3. Catalytic performance of the 3D network, pure ZIF-8 nanocrystals and ZIF-8 microcrystals as a function of time.

The 3D network with a loose structure has an optimum structure to catalyze reactions on its external surface because most of the external surface in the 3D network of the composite nanowires, which were very large because of the small diameter of the nanowires, was exposed to the macropores (Figure 1b and Figure S2c and e). Moreover, the mesopores derived from gaps between neighboring nanocrystals on ZIF-8 crystal layer would further increase the external surface for catalytic reactions. To demonstrate efficient catalysis, the 3D network was used to catalyze the Knoevenagel reaction between benzaldehyde and malononitrile (the mechanism see S8 in the ESI) and the results were compared to those obtained using pure ZIF-8 nanocrystals (65 nm) and ZIF-8 microcrystals (1 μm) to catalyze the same reaction (Figure S10). All three types of ZIF-8 materials were prepared in methanol and purified and activated through the same process and under the same conditions. As indicated in Figure 2b, both the microsized and nanosized ZIF-8 crystals are perfect in the crystallinity. The 3D network exhibited the highest catalytic activity among the three catalysts. As evident in Figure 3, at the same catalyst-to-reactants weight ratio, the reaction conversion after 10 h was 63% for the 3D network, but only 45% and 30% for the pure ZIF-8 nano- and micro- crystals, respectively. The product of this reaction is benzalmalononitrile and the selectivity are 91.8%, 86.6% and 88.4% respectively. The kinetic diameters of

benzaldehyde and malononitrile were 0.60 nm and 0.43 nm, respectively, which are larger than the micropore size of ZIF-8 (0.34 nm). The molecules could therefore not enter the micropores, and the catalytic reaction could only occur on the external surface of ZIF-8.[12] Compared with the ZIF-8 nanocrystals, the 3D network was constructed from the composite nanowires that had a uniform width of 60 nm and thus a larger specific external surface area. Moreover, the 3D network formed from the crosslinking had a large amount of macropores to which most of the external surface of the nanowires was exposed, making most of the active external surface easy to access. In the ZIF-8 nanocrystals, fusion between the particles inevitably occurred during purification and activation, leading to the loss of a considerable portion of the external surface and of continuity in the pores. These losses could account for the superior catalytic activity of the 3D network over that of the ZIF-8 nanocrystals. The ZIF-8 microcrystal exhibited the lowest catalytic activity because its specific external surface area was the lowest among the investigated catalysts.

In summary, we have successfully prepared a 3D network constructed with 1D ZIF-8-coated, PW-composite nanowires through a solution-based method that can be used to easily fabricate gram quantities of product. In the reaction mixture, the precursors of ZIF-8 interacted with PWs and crystallized to form a ZIF-8 layer surrounding the PWs, and the fusion between the primary crystals crosslinked the individual nanowires to form the 3D network. This 3D network had a loose structure containing micropores, mesopores and macropores and exhibited high catalytic activity when used to catalyze the Knoevenagel reaction between benzaldehyde and malononitrile.

We are grateful for the financial support of NSFC (21334001) and the Ministry of Science and Technology of China (2011CB932503)

Notes and references

Junqi Yi and Haodong Li contributed equally to this work.

Note 1. The MOFs with a large specific external surface area and the external surface being fully exposed are highly desirable, because such MOFs can enable fast mass transfer within them and access by large molecules. Besides, since the Lewis acidic/basic sites on the external surface are unsaturated and can function as active points, preparing the large and fully exposed external surface will remarkably increase the activities of the MOFs, especially those for interacting with (e.g., catalyzing or adsorbing) large molecules.

1. (a) M. Kondo, T. Yoshitomi, H. Matsuzaka, S. Kitagawa and K. Seki, *Angewandte Chemie International Edition in English*, 1997, **36**, 1725-1727; (b) H. Li, M. Eddaoudi, M. O'Keeffe and O. M. Yaghi, *Nature*, 1999, **402**, 276-279.
2. (a) N. L. Rosi, J. Eckert, M. Eddaoudi, D. T. Vodak, J. Kim, M. O'Keeffe and O. M. Yaghi, *Science*, 2003, **300**, 1127-1129; (b) K. Sumida, D. L. Rogow, J. A. Mason, T. M. McDonald, E. D. Bloch, Z. R. Herm, T.-H. Bae and J. R. Long, *Chemical Reviews*, 2012, **112**, 724-781.
3. J. B. DeCoste and G. W. Peterson, *Chemical Reviews*, 2014, **114**, 5695-5727.
4. J.-R. Li, J. Sculley and H.-C. Zhou, *Chemical Reviews*, 2012, **112**, 869-932.
5. A. Corma, H. García and F. X. Llabrés i Xamena, *Chemical Reviews*, 2010, **110**, 4606-4655.
6. L. E. Kreno, K. Leong, O. K. Farha, M. Allendorf, R. P. Van Duyne and J. T. Hupp, *Chemical Reviews*, 2012, **112**, 1105-1125.
7. (a) A. Carne, C. Carbonell, I. Imaz and D. Maspoch, *Chemical Society Reviews*, 2011, **40**, 291-305; (b) R. Ostermann, J. Cravillon, C. Weidmann, M. Wiebcke and B. M. Smarsly, *Chemical Communications*, 2011, **47**, 442-444; (c) N. Stock and S Biswas, *Chemical Reviews*, 2012, **112**, 933-969; (d) V. Valtchev and L. Tosheva, *Chemical Reviews*, 2013, **113**, 6734-6760; (e) X. Fan, W. Wang, W. Li, J. Zhou, B. Wang, J. Zheng and X. Li, *ACS Applied Materials & Interfaces*, 2014, **6**, 14994-14999; (f) S. Furukawa, J. Reboul, S. Diring, K. Sumida and S. Kitagawa, *Chemical Society Reviews*, 2014, **43**, 5700-5734.
8. (a) O. Shekhah, J. Liu, R. A. Fischer and C. Woll, *Chemical Society Reviews*, 2011, **40**, 1081-1106; (b) H. Du, J. Bai, C. Zuo, Z. Xin and J. Hu, *CrystEngComm*, 2011, **13**, 3314-3316; (c) A. Carné-Sánchez, I. Imaz, M. Cano-Sarabia and D. Maspoch, *Nat Chem*, 2013, **5**, 203-211.
9. S. Cao, G. Gody, W. Zhao, S. Perrier, X. Peng, C. Ducati, D. Zhao and A. K. Cheetham, *Chemical Science*, 2013, **4**, 3573-3577.
10. (a) K. M. Choi, H. J. Jeon, J. K. Kang and O. M. Yaghi, *Journal of the American Chemical Society*, 2011, **133**, 11920-11923; (b) W. Xuan, C. Zhu, Y. Liu and Y. Cui, *Chemical Society Reviews*, 2012, **41**, 1677-1695; (c) L.-B. Sun, J.-R. Li, J. Park and H.-C. Zhou, *Journal of the American Chemical Society*, 2012, **134**, 126-129; (d) L. Peng, J. Zhang, J. Li, B. Han, Z. Xue and G. Yang, *Chemical Communications*, 2012, **48**, 8688-8690; (e) B. Tu, Q. Pang, D. Wu, Y. Song, L. Weng and Q. Li, *Journal of the American Chemical Society*, 2014, **136**, 14465-14471.
11. K. S. Park, Z. Ni, A. P. Côté, J. Y. Choi, R. Huang, F. J. Uribe-Romo, H. K. Chae, M. O'Keeffe and O. M. Yaghi, *Proceedings of the National Academy of Sciences*, 2006, **103**, 10186-10191.
12. U. P. N. Tran, K. K. A. Le and N. T. S. Phan, *ACS Catalysis*, 2011, **1**, 120-127.
13. (a) K. Zhang, M. Jiang and D. Chen, *Angewandte Chemie International Edition*, 2012, **51**, 8744-8747; (b) K. Zhang, J. Yi and D. Chen, *Journal of Materials Chemistry A*, 2013, **1**, 14649-14657; (c) K. Zhang, H. Miao and D. Chen, *Journal of the American Chemical Society*, 2014, **136**, 15933-15941.
14. (a) T. Tsuruoka, S. Furukawa, Y. Takashima, K. Yoshida, S. Isoda and S. Kitagawa, *Angewandte Chemie International Edition*, 2009, **48**, 4739-4743; (b) A. Aerts, M. Haouas, T. P. Caremans, L. R. A. Follens, T. S. van Erp, F. Taulelle, J. Vermant, J. A. Martens and C. E. A. Kirschhock, *Chemistry – A European Journal*, 2010, **16**, 2764-2774; (c) J. Cravillon, C. A. Schröder, R. Nayuk, J. Gummel, K. Huber and M. Wiebcke, *Angewandte Chemie International Edition*, 2011, **50**, 8067-8071.
15. H.-P. Lin, S.-T. Wong, C.-Y. Mou and C.-Y. Tang, *The Journal of Physical Chemistry B*, 2000, **104**, 8967-8975.
16. (a) N. Liu, Y. Yao, J. Cha, M. McDowell, Y. Han and Y. Cui, *Nano Res.*, 2012, **5**, 109-116; (b) R. Jin, Z. Bian, J. Li, M. Ding and L. Gao, *Dalton Transactions*, 2013, **42**, 3936-3940; (c) F. Zhang, Y. Wei, X. Wu, H. Jiang, W. Wang and H. Li, *Journal of the American Chemical Society*, 2014, **136**, 13963-13966.
17. (a) J. Cravillon, S. Münzer, S.-J. Lohmeier, A. Feldhoff, K. Huber and M. Wiebcke, *Chemistry of Materials*, 2009, **21**, 1410-1412; (b) J. Cravillon, R. Nayuk, S. Springer, A. Feldhoff, K. Huber and M. Wiebcke, *Chemistry of Materials*, 2011, **23**, 2130-2141.

